CAD-based topology optimization system with dynamic feature shape and modeling history evolution

Jikai Liu[1,2,3], Albert C. To[3,*]

[1]Center for Advanced Jet Engineering Technologies (CaJET), Key Laboratory of High Efficiency and Clean Mechanical Manufacture (Ministry of Education), School of Mechanical Engineering, Shandong University, Jinan, China

[2]Key National Demonstration Center for Experimental Mechanical Engineering Education, Shandong University, Jinan, China

[3]Department of Mechanical Engineering and Materials Science, University of Pittsburgh, Pittsburgh, Pennsylvania 15261, USA

*Corresponding author. Email: albertto@pitt.edu

Abstract

Conventional topology optimization presentations generally highlight the numerical and optimization details established on the specially-customized discrete geometric modeling system, which is incompatible with the existing CAD/CAE systems. Therefore, tedious pre- and post-processing are required to improve the editability and manufacturabilitym, which are both time-consuming and labour-intensive. Hence, to address this challenging issue, a novel CAD-based topology optimization system is developed in this work. The following points are highlighted: (i) Interoperability issue between CAD and topology optimization was addressed by using macro files to communicate the feature and modeling history information; then, (ii) structural shape and topology optimization is performed based on a B-spline-based approach, which inherits the original spline information from the upstream CAD model and of course, can return spline-based geometric information for optimized CAD model generation; and the last but the most important point to mention is that, (iii) modeling history was incorporated into the optimization process and dynamic modeling history change is enabled based on the optimality criteria. This final point is significant because history-based CAD modeling is still a main-stream approach, especially given the excellent post-modeling editability and design intent capture.

Keywords: Topology optimization; B-spline; Dynamic modeling history; Interoperability

1. Introduction

Topology optimization is a computational design method to automatically distribute a certain amount of materials within the given design domain to achieve the desired structural performance. Since first proposed in 1988 [1], topology optimization has undergone extensive development and now, it is widely accepted by industry and has been applied to a wide range of structural optimization problems subject to different physical disciplines [2], such as multi-material design [3–9], casting part design [10,11], additive manufacturing part design [12–22], robust design [23–26], and many others [27,28]. On the other hand, some inherent problems were there from the beginning and have complicated the application of topology optimization, e.g., the poor compatibility to the current CAD/CAM system, which will be addressed in this research work. In general, density-based topology optimization adopts the discrete voxel model for geometry representation, which is flexible for handling both shape and topological changes. However, it goes against the parameterized model representation (spline-based) in CAD. Tremendous efforts [29–37] have been made to parameterize the topology optimization results using spline functions. These days, this type of post-optimization surface smoothing and parameterization has been supported by commercial topology optimization packages, i.e., having the output in IGES or STEP format [38]. At the same time, a more aggressive approach is to directly conduct topology optimization using B-spline based geometry representation [39–45]. Thus far, it is trivial to obtain a parameterized, readable CAD model as the topology optimization output [46]. However, it is far from enough to only ensure the readability. Within the product development lifecycle, topology optimization is typically done at the very early conceptual design stage solely for structural design purpose. It is conceptual without considering many product lifecycle related issues [47], e.g., functionality, manufacturability, assembility, etc. Therefore, it is of critical importance to have an editable CAD model from topology optimization output, so that engineers from different departments can perform post-optimization editing through CAD/CAM/CAPP (Computer Aided Process Planning), or other CAx (Computer Aided Technology) software tools. However, existing software tools

generally perform poorly in converting topology optimization result into an editable CAD model. Re-modeling has to be conducted by the design engineer manually. For the reason, commercial CAD platforms mainly support feature-based and history-driven geometric modeling, where geometric feature primitives are combined through a sequence of Boolean operations (recorded as the modeling history). However, existing topology optimization methods do not involve the history concept, even though there exist feature-based or feature-involved topology optimization methods [48–57].

Based on the above discussion, the main objective of this research work is to address the compatibility issue of topology optimization with CAD. And the basic idea is to develop a CAD-based topology optimization method, i.e., start with a history-based CAD model as the input, transform the geometric representation into a CAD software-independent and optimization-friendly neutral format, perform topology optimization, finally change the geometric representation back into its original format (commercial CAD system compatible). To close this loop, many specific issues should be addressed and the technical details will be introduced below:

Interchangeability between CAD and Optimization. Conventionally, interoperability of CAD models among different CAD systems is problematic, since CAD systems generally have their proprietary geometric formats and additional efforts are required to make the translation, for example, generating neutral formats such as IGES and STEP. However, IGES and STEP only convey the geometric information. The model at the receiving CAD system is frozen due to loss of the design intent (modeling history, geometric constraints, and many others). To address this issue, many other neutral formats have been proposed to realize history-based CAD model translation among different CAD systems, such as the macro file based neutral model [58–62]. Since this issue is not specifically targeted in this work, the technical pros and cons of the different neutral formats will not be discussed here. For the sake of simplicity, the macro file will be employed in this research as a tool to communicate between CAD and the optimization module. In addition, between the standard macro file and topology optimization, one more translation is needed to

transform the explicit geometric information in CAD into the implicit representation for topology optimization to handle potential topological changes; refer to Fig. 1 for the schematic illustration.

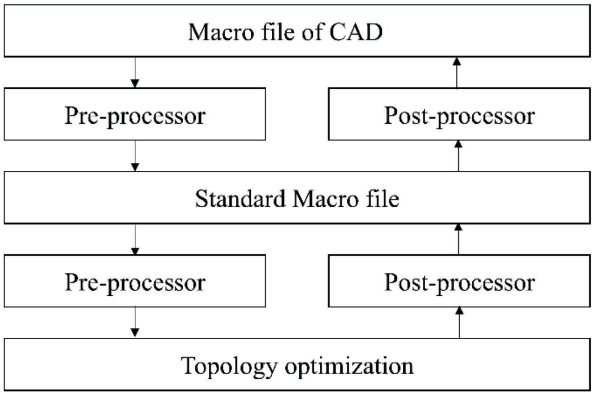

Fig. 1 System framework

B-spline based topology optimization. Once the geometric model is transformed into the implicit B-spline representation (or NURBS), the model turns into CSG (Constructive Solid Geometry) format which can trivially handle any shape and topological changes. Then, the structural shape and topology optimization will be performed based on the implicit B-spline based level set method [42,43]. Note that, there could have design intent stored in the original CAD model in different forms, such as geometric constraints and semantic properties. However, interpretation of the geometric constraints and semantic properties would over-complicate the optimization problem, and thus will not be considered in the current paper. It will be explored in future work.

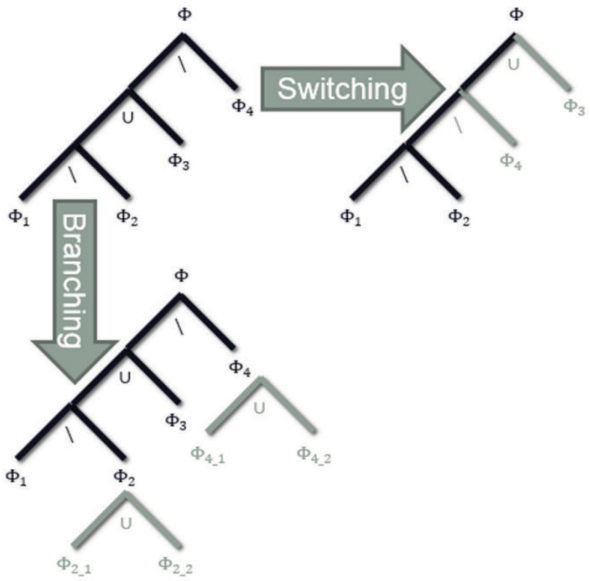

Fig. 2 Modeling history topological change

Modeling history topological change. The topology optimization method proposed in this work contributes an important technique for handling modeling history topological changes. Here, the modeling history topological change means changes of the hierarchical modeling history tree; see Fig. 2. Obviously, performing topology optimization subject to a fixed modeling history only yields a sub-optimal solution. Allowing changes in the Boolean operation sequence expands the design space which therefore can lead to a better design solution. However, such kind of modeling history topological changes conventionally are not considered. This motivates the idea of incorporating dynamic modeling history evolution into topology optimization. So far, two types of modeling history topological changes are considered; see Fig. 2, and specific algorithms have been developed to handle such types of topological changes.

In summary, the CAD-based topology optimization method proposed in this research made contribution to the field in the following aspects:

1) For the first time, the CAD-based topology optimization method is realized, in which we start from a CAD model as the input and end up with an editable CAD model as the output. The output is compatible to the main-stream history-based feature modeling scenario of most commercial CAD packages.

Beneficially, the often-employed manual CAD model reconstruction can be eliminated, which saves labor and also guarantees accuracy of the model reconstruction.

2) Also for the first time, two different types of topological changes have been concurrently addressed of both geometric topological changes and modeling history topological changes, which guarantees exploration of a large enough design space.

2. Interchangeability between CAD and optimization

As a CAD-based topology optimization method, the proposed algorithm starts from a CAD model input, optimizes the feature parameters (sizing parameters of regular shapes and control points of freeform shapes) and the modeling history, and finally returns the optimized design as a valid and editable CAD model, as demonstrated in Fig. 1. In this paper, script file of the open-source CAD modeling tool OpenSCAD is used as the input (Macro file input). Communication of both the feature information and sequence of the Boolean operations (modeling history) has been realized to seamlessly integrate CAD with our in-house topology optimization code. Therefore, a closed loop of CAD-based topology optimization has been achieved. Figure 3 demonstrates an example of the script-based CAD modeling in OpenSCAD. This type of script-based modeling is supported by most of the CAD systems, while complexity of the script structure differs significantly. OpenSCAD is used in this research for the sake of simplicity.

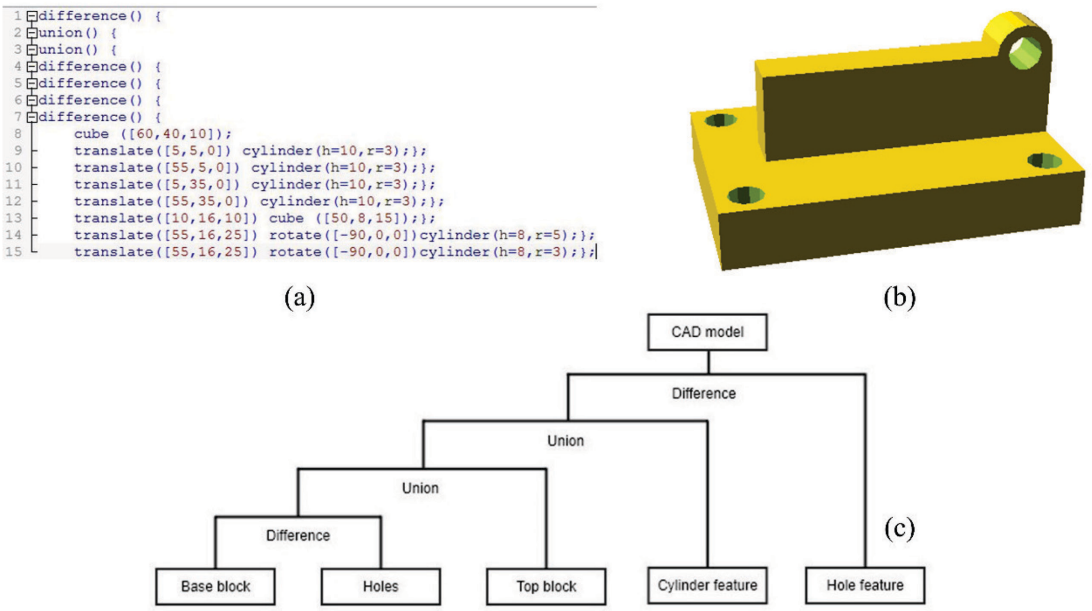

Fig. 3 Script-based CAD modeling in OpenSCAD: (a) Modeling script; (b) CAD model; (c) Modeling history

3. Closed B-spline based 2.5D machining feature representation

3.1 B-spline profile representation

B-spline models the curve through a linear combination of the control points $\mathbf{P}_i$ and B-spline basis functions $N_{i,k}(t)$.

$$\mathbf{P}(t) = \sum_{i=0}^{n} \mathbf{P}_i \, N_{i,k}(t)$$

$$N_{i,0}(t) = \begin{cases} 1, & if\ t_i \le t < t_{i+1} \\ 0, & otherwise \end{cases} \tag{1}$$

$$N_{i,j}(t) = \frac{t - t_i}{t_{i+j} - t_i} N_{i,j-1}(t) + \frac{t_{i+j+1} - t}{t_{i+j+1} - t_{i+1}} N_{i+1,j-1}(t)$$

$$j = 1,2,\dots,k$$

where k is the order of the curve. $\mathbf{T} = [t_0, t_1, \ldots, t_m]$ is the knot vector with the non-decreasing sequence with $t_i \in [0,1]$, and $m = n + 1 + k$. Figure 4 demonstrates the quadratic B-spline basis functions ($n = 6$) with different knot vectors.

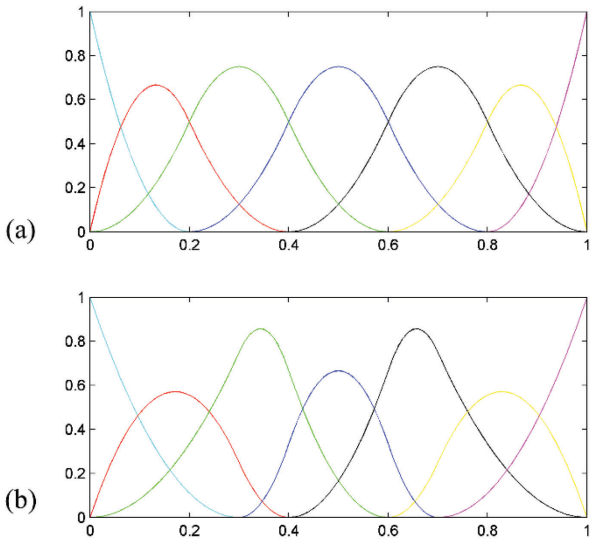

Fig. 4 Quadratic B-spline basis functions ($n = 6, k = 2$) with the knot vector of: (a) $\mathbf{T} =$ [0,0,0,0.2,0.4,0.6,0.8,1,1,1] and (b) $\mathbf{T} = [0,0,0,0.3,0.4,0.6,0.7,1,1,1]$

Then, the internal space formed by the closed B-spline is represented by Eq. (2),

$$\Phi = r(\theta) - \sqrt{(x - x_0)^2 + (y - y_0)^2}$$

$$r(\theta) = \sum_{i=0}^{n} R_i \, N_{i,k}\left(\frac{\theta + \frac{\pi}{2}}{2\pi}\right) \tag{2}$$

$$\theta = acrtan\frac{y - y_0}{x - x_0} + \pi \cdot H(x_0 - x)$$

where $H(\cdot)$ is the Heaviside function, and $\mathbf{R}$ is the vector of control parameters. To ensure the closure, the same value is assigned to the R_i of the starting and ending points.

In fact, Equation (2) can be regarded as a level set description of the geometry, where the general expression is presented in Eq. (3).

$$\begin{cases} \Phi(\mathbf{X}) > 0, & \mathbf{X} \in \Omega / \partial\Omega \\ \Phi(\mathbf{X}) = 0, & \mathbf{X} \in \partial\Omega \\ \Phi(\mathbf{X}) < 0, & \mathbf{X} \in D/\Omega \end{cases} \tag{3}$$

where Ω represents the material domain, D indicates the entire design domain, and D/Ω represents the void.

Figure 5a presents the closed B-spline with $\mathbf{R} = [1.5, 3, 1, 2, 3.5, 2, 1.5]$ and the same B-spline basis function as shown in Fig. 4a. In Fig. 5b, by making $R_1 = R_7 = (R_2 + R_6)/2$, the poor continuity condition at the end point is relieved.

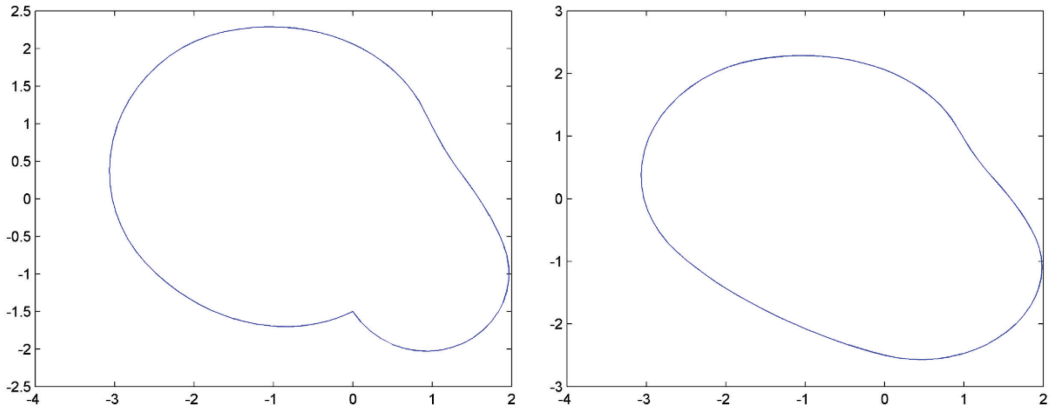

(a) (b)

Fig. 5 Closed B-spline

3.2 Constructive description of the part

Individual features can be represented by extruding the closed B-spline profiles. Then, CSG (constructive solid geometry) modeling is adopted for CAD geometry construction, which combines the implicitly represented individual features through a sequence of Boolean operations. CSG modeling has the advantage of being insensitive to topological changes [63] compared to the B-rep (Boundary representation) model, which therefore, has often been adopted for structural shape and topology optimization [48,49].

Specifically, the commonly used Boolean operations are demonstrated in Eq. (4).

$$\Phi_1 \cup \Phi_2 = max(\Phi_1, \Phi_2), \quad Unite$$
$$\Phi_1 \cap \Phi_2 = min(\Phi_1, \Phi_2), \quad Intersect \tag{4}$$
$$\Phi_1 \setminus \Phi_2 = min(\Phi_1, -\Phi_2), \quad Substract$$

For instance, the constructive history of a bracket part as shown in Fig. 6 is illustrated in Eq. (5), where the parametric level set descriptions of the involved feature primitives are demonstrated.

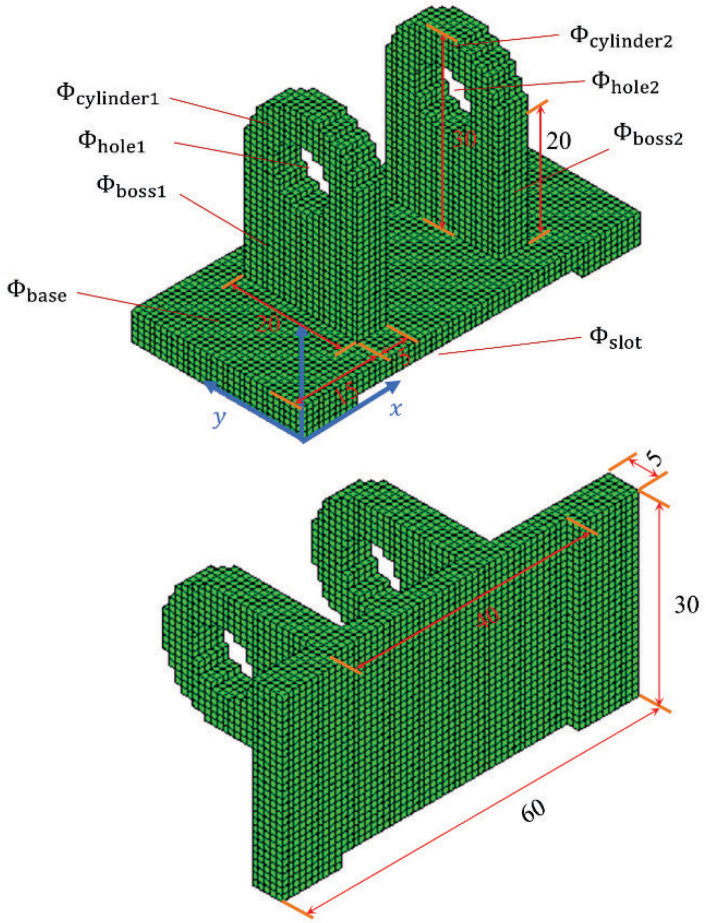

Fig. 6 Constructive description of the bracket

$$\Phi = (\Phi_{\text{cylinder1}} \cup \Phi_{\text{boss1}} \backslash \Phi_{\text{hole1}}) \cup (\Phi_{\text{cylinder2}} \cup \Phi_{\text{boss2}} \backslash \Phi_{\text{hole2}}) \cup (\Phi_{\text{base}} \backslash \Phi_{\text{slot}})$$

$$\Phi_{\text{cylinder1}} = \min\left\{10 - [(y-15)^2 + (z-25)^2]^{\frac{1}{2}}, min(x-15{,}20-x)\right\}$$

$$\Phi_{\text{hole1}} = \min\left\{5 - [(y-15)^2 + (z-25)^2]^{\frac{1}{2}}, min(x-15{,}20-x)\right\}$$

$$\Phi_{\text{boss1}} = \min\{2.5-(x-17.5), 2.5+(x-17.5), 10-(y-15), 10+(y-15),$$
$$10-(z-15), 10+(z-15)\} \tag{5}$$

$$\Phi_{\text{cylinder2}} = \min\left\{10 - [(y-15)^2 + (z-25)^2]^{\frac{1}{2}}, min(x-40{,}45-x)\right\}$$

$$\Phi_{\text{hole2}} = \min\left\{5 - [(y-15)^2 + (z-25)^2]^{\frac{1}{2}}, min(x-40{,}45-x)\right\}$$

$$\Phi_{\text{boss2}} = \min\{2.5-(x-42.5), 2.5+(x-42.5), 10-(y-15), 10+(y-15),$$
$$10-(z-15), 10+(z-15)\}$$

$$\Phi_{\text{base}} = \min\{30-(x-30), 30+(x-30), 15-(y-15), 15+(y-15),$$
$$2.5-(z-2.5), 2.5+(z-2.5)\}$$

$$\Phi_{\text{slot}} = \min\{20-(x-30), 20+(x-30), 15-(y-15), 15+(y-15),$$
$$1-(z-1), 1+(z-1)\}$$

3.3 Optimization problem and its solution

Then, compliance-minimization topology optimization problem on B-spline based CSG model is formulated below:

$$\begin{aligned} &Min. \quad J\left(\boldsymbol{\Phi}, \overline{\boldsymbol{\Phi}}\right) = \int_D \mathbf{De}(\mathbf{u})\mathbf{e}(\mathbf{u})H(\Phi)d\Omega \\ &s.t. \quad a\left(\mathbf{u}, \mathbf{v}, \boldsymbol{\Phi}, \overline{\boldsymbol{\Phi}}\right) = l(\mathbf{v}), \qquad \forall \mathbf{v} \in U_{ad} \end{aligned} \tag{6}$$

$$\int_D H(\Phi)d\Omega \le V_{max}$$

$$a\left(\mathbf{u},\mathbf{v},\boldsymbol{\Phi},\overline{\boldsymbol{\Phi}}\right) = \int_D \mathbf{De}(\mathbf{u})\mathbf{e}(\mathbf{v})H(\Phi)d\Omega$$

$$l(\mathbf{v}) = \int_D \mathbf{p}\cdot\mathbf{v}d\Omega + \int_\Gamma \boldsymbol{\tau}\cdot\mathbf{v}dS$$

in which $a(\quad)$ is the energy bilinear form and $l(\quad)$ is the load linear form. $\mathbf{u}$ is the deformation vector, $\mathbf{v}$ is the test vector, and $\mathbf{e}(\mathbf{u})$ is the strain. $U = \{\mathbf{v} \in H^1(\Omega)^d | \mathbf{v} = 0 \; on \; \Gamma_D\}$ is the space of kinematically admissible displacement field. $\boldsymbol{p}$ is the body force and $\boldsymbol{\tau}$ is the boundary traction force, which are assumed not spatially varying. V_{max} is the upper bound of the material volume fraction. $\boldsymbol{\Phi}, \overline{\boldsymbol{\Phi}}$ represent the parametric level set functions and B-spline based level set functions, respectively. Φ indicates the resulting constructed level set field.

The sensitivity result is well known as presented in Eq. (7) [64,65]:

$$\begin{aligned} L' &= \int_D R\delta(\Phi)\Phi'|\nabla\Phi|d\Omega \\ R &= -\mathbf{De}(\mathbf{u})\mathbf{e}(\mathbf{u}) + \lambda \end{aligned} \tag{7}$$

where λ is the Lagrange multiplier, and the approximated Dirac Delta function in [64] is employed.

$$\frac{\partial\Phi}{\partial R_i} = \frac{\partial\Phi}{\partial\overline{\Phi}_j}\frac{\partial\overline{\Phi}_j}{\partial R_i} = \begin{cases} N_{i,k}\left(\dfrac{\theta+\frac{\pi}{2}}{2\pi}\right) & if\ \Phi = \overline{\Phi}_j \\ 0 \quad if\ \Phi \ne \overline{\Phi}_j \end{cases} \tag{8}$$

where $\overline{\Phi}_j$ is the jth B-spline represented design feature. Details of the sensitivity analysis have been well demonstrated in [41,43], so that will not be further repeated.

Accordingly, a numerical example is explored below. The finite element analysis (FEA) is performed based on fixed hexahedral mesh and the artificial weak material is employed for voids to avoid the stiffness matrix singularity, which is:

$$\mathbf{D}_{\mathrm{v}} = 10^{-3}\mathbf{D} \tag{9}$$

in which $\mathbf{D}_{\mathrm{v}}$ is the elasticity tensor of the void. Stiffness of any boundary-crossed element is determined by $\rho\mathbf{D}$, wherein ρ represents the solid material volume fraction of the boundary-cut element.

The volume constraint is addressed by the Augmented Lagrange multiplier, as presented in Eq. (10).

$$\lambda_{k+1} = \max\left[0, \lambda_k + \frac{1}{\mu_k}\left(\int_D H(\Phi)d\Omega - V_{max}\right)\right]$$
$$\mu_{k+1} = \alpha\mu_k \;\; where \; 0 < \alpha < 1 \tag{10}$$

in which μ is the penalization factor and α is its adjustment parameter.

For this cantilever problem, the design domain (60*30*10) and boundary conditions are demonstrated in Fig. 7a. The left side wall is fixed and the uniform forces of magnitude 0.1 per distance are imposed on the right bottom edge. As shown in Fig. 7(b-c), eight through-hole features and three step-hole features are deployed inside the design domain, acting as the moving fronts of the shape and topology evolution. Note that, only the front half of the cantilever structure is demonstrated because of symmetry. The solid material employs a Young's modulus value of 1 and Poison's ratio value of 0.3. The optimization problem is to minimize the structural compliance under the maximum material volume fraction of 0.5.

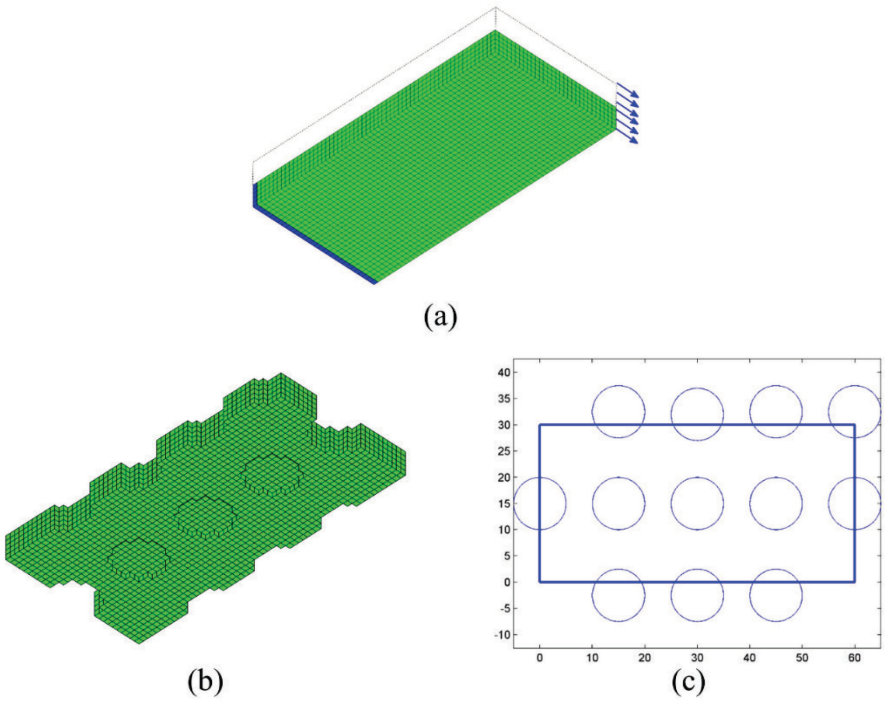

Fig. 7 Initial guess of the topology optimization problem: (a) Design domain and boundary conditions (only the front half is demonstrated of size 60*30*5); (b) Initially deployed machining features; (c) The closed B-spline curves in 2D view

The optimization result is shown in Figure 8. We can see that even though only extrusion features are included, there is enough design freedom to derive the optimization result close to the conventional topological design. It can be seen from Fig. 8 that the algorithm suffers from the issue of non-smooth intersection cusps. Actually in [41], this problem has been solved by creating new B-spline profiles by merging the intersecting ones. However, this type of approach cannot be directly realized, since the underlying formulas of merging B-spline profiles of commercial CAD packages are forbidden to users that cannot be addressed in the optimization code. Therefore, this issue can be solved with a straightforward approach by rounding the cusps as a post-processing, since rounding is a standard function in all commercial CAD packages that can be realized with a single line of code in the Macro file.

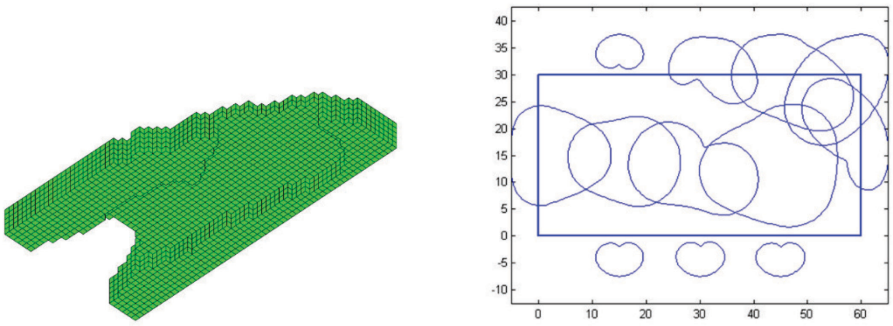

Fig. 8 The topology optimization result (objective value = 13.47): (a) Initially deployed machining features; (b) The closed B-spline curves in 2D view

4. Topology optimization with dynamic modeling history

The numerical example presented in Sec. 3 only involves difference Boolean operation, the result of which would not be affected by the sequence of Boolean operations. However, in a more general situation where different kinds of Boolean operations are included, the modeling history-dependency issue would emerge. In other words, the optimization result is strongly dependent on the modeling history even if the same initial geometry is adopted. Given the reason, the same set of feature primitives constructed with different set of Boolean operations could form the same geometry, but with the gradual feature shape evolution, the constructed geometries cannot be guaranteed always the same. There has a high possibility that the optimized designs would be different due to the different modeling histories. It is impossible to determine the best modeling history at the initial guess, which results in the local optimum issue.

Another issue worth mentioning is that, topology optimization characterizes in deriving complex geometries from simple initial guesses. However, if modeling history is involved, the modeling history will be consistent throughout the optimization and thus, the structural complexity would not vary too much due to the restricted amount of 2.5D features. It means optimization with simple initial guesses will end up with something simple as well. This is good from some perspective such as low manufacturing cost, but can also be negative since the design space is severely restricted. Hence, it is necessary to provide some mechanism

for the algorithm to increase the modeling history complexity, i.e., add more nodes to the modeling history tree.

In summary, this paper proposes a new concept of modeling history topological change to address the afore-mentioned two issues. Two types of modeling history topological changes are proposed: the switching and branching topological changes. More details will be presented at the rest of this section.

4.1 Switching topological change

Figure 9 demonstrates a history-based CAD modeling process and the related structural optimization result with a consistent modeling history. This is a cantilever problem, where the left-side wall is clamped with zero displacement and a point force pointing downwards is loaded at the center of the right surface. The four slot features (highlighted in red) are designable and their cross-section profiles (perpendicular to the extrusion direction) are transformed into closed B-spline representations.

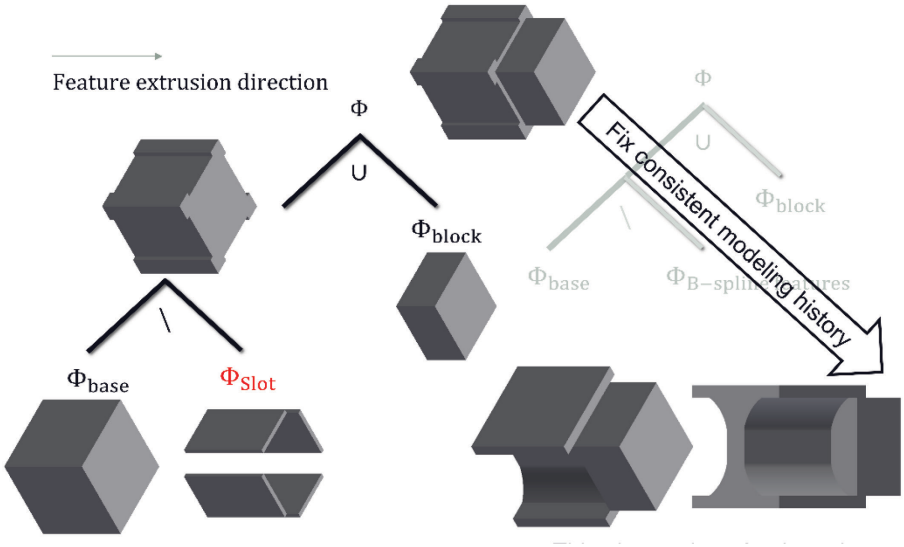

Fig. 9 Optimization with a fixed modeling history

The optimization result in Fig. 9 is very likely only a sub-optimal, since it goes against our intuition on the I-beam like cantilever structure. The design space is restricted by the fixed modeling history. Therefore, to achieve the modeling history-independency effect, we propose the modeling history topological derivative

(MHTD) and integrate it with the B-spline based topology optimization algorithm. The MHTD is mathematically different from the conventional topological derivative concept [66–68] but more closely related to the shape derivative concept. It does not indicate the tearing or splitting-type structural topological changes; rather, the terminology 'modeling history topological derivative' stems from topological changes of the hierarchical modeling history tree structure, which belongs to another type of topological change particularly important for CAD modeling. Physically, the MHTD evaluates the effect of Boolean operation sequence switch on the objective function.

Consider the compliance minimization problem of Eq. (6). Assume Φ to be the level set function constructed with the current modeling history and $\widetilde{\Phi}$ to be the level set function with the modified modeling history. Then, the impact of switching the modeling history can be evaluated using the following equation:

$$L\left(\widetilde{\Phi}\right) - L(\Phi) = J\left(\widetilde{\Phi}\right) - J(\Phi) + \bar{\lambda}\left(V\left(\widetilde{\Phi}\right) - V(\Phi)\right)$$

$$= \int_D \left(-\mathbf{De}(\mathbf{u})\mathbf{e}(\mathbf{u}) + \bar{\lambda}\right)\delta(\Phi)\Phi' d\Omega \tag{11}$$

$$\Phi' = \widetilde{\Phi} - \Phi$$

Since the Lagrangian should always decrease, modeling history switch will happen only if a negative value is obtained from Eq. (11). Additionally, since only the first order derivative information is available, the switch judgement will only be calculated in case of a minor volume fraction change, i.e., $|V\left(\widetilde{\Phi}\right) - V(\Phi)| \leq \varepsilon$, where ε is a small positive number.

One more important issue is that the result of Eq. (11) will be severely affected by the Lagrange multiplier value. Because of the adopted augmented Lagrange multiplier method, the Lagrange multiplier changes in an iterative basis according to the satisfaction of the inequality constraint. Hence, the result of Eq. (11) will not be robust and can be affected by many factors such as the initial guess of the Lagrange multiplier and

the penalization term. In order to avoid this problem, an alternative approach [64] based on the KKT condition is adopted to calculate this Lagrange multiplier as shown below:

$$\bar{\lambda} = \frac{\int_D \mathbf{De}(\mathbf{u})\mathbf{e}(\mathbf{u})\delta(\Phi)|\nabla\Phi|d\Omega}{\int_D \delta(\Phi)|\nabla\Phi|d\Omega} \tag{12}$$

With this calculation method, the Lagrange multiplier only depends on the strain energy distribution at the evolving surface, which functions to reduce materials at the below-average areas and increase materials at the above-average areas. The augmented Lagrange multiplier, the penalization term, and the satisfaction condition of the inequality constraint would no longer affect the calculation of Eq. (11). Note that, an over bar is used to distinguish this Lagrange multiplier with the augmented Lagrange multiplier used for regular design update.

Given a modeling history, there are many possibilities of switching and a few rules have been defined to guide the switch operations. (i) Only the B-Spline features (designable features) will be considered to change its position in the modeling history structure. (ii) Each B-spline feature primitive has two directions to switch, either upwards or downwards (one direction if at the top or bottom layer of the tree structure). (iii) Only the switch of two different types of Boolean operations is effective, since switch of two union or difference operations would not cause any structural shape change. All the potential switches that satisfy the above three requirements will be evaluated. Therefore, in case of N switchable feature primitives, at most $2N$ times of MHTD calculations are needed in each optimization loop. Calculation of Eq. (11) is trivial which would not affect the overall computational efficiency. The costly FEA is only performed once in each loop.

Figure 10 demonstrates the different result if MHTD is involved. Switch of the union and difference operations happens in an intermediate step which leads to a different design as compared with Figure 8 and also a further compliance reduction of 10.37 percent.

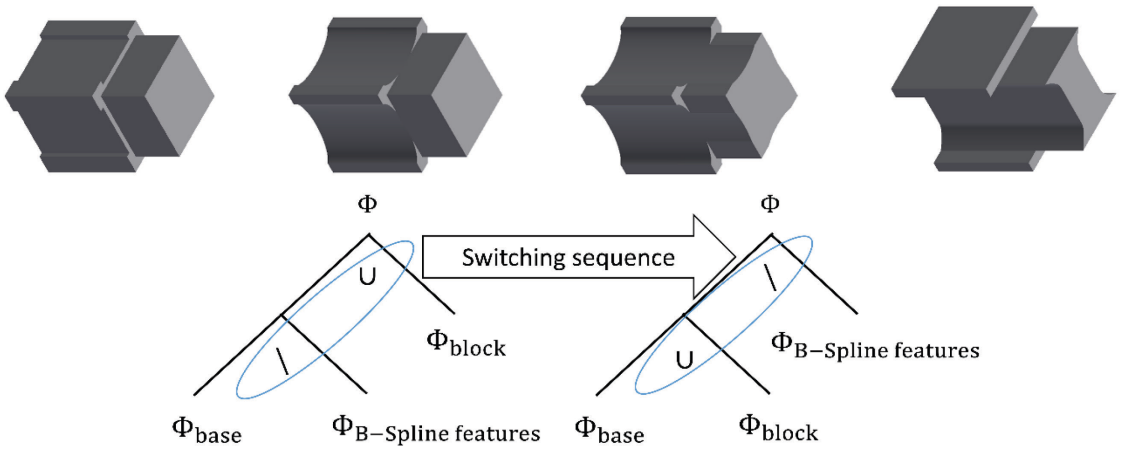

Fig. 10 Optimization with Boolean operation switch

4.2 Branching topological change

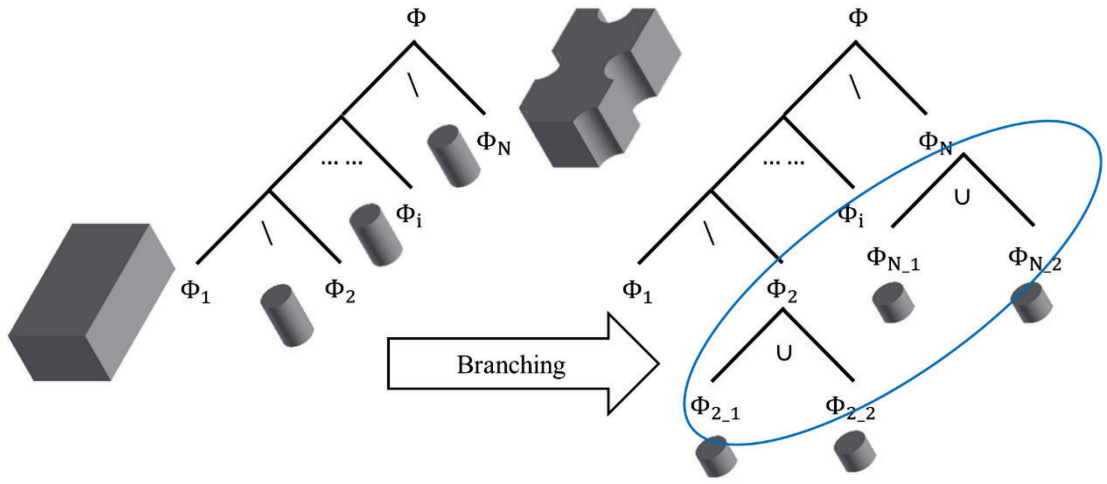

Fig. 11 Illustration of the branching topological change

Figure 11 illustrates the idea of branching topological change, i.e., one primitive feature element (e.g. Φ_2) is divided into two (e.g. Φ_{2_1} and Φ_{2_2}), so that the cross-section profile of the original feature element is divided into two profiles that can independently evolve, which apparently increases the design space. On

the other hand, the CAD model complexity increases with the branching topological change, which leads to difficulties of managing the CAD model and also manufacturing. Hence, it is a desirable feature to performing branching topological changes from the perspective of mechanical performance enhancement. On the other hand, there should be a criterion to stop the branching, because otherwise, the endless branching operations will make both the computational and manufacturing costs too high. Similar to [48], the feature volume could be an appropriate measure to qualify the branching operation, i.e., only the feature primitives that have a feature volume larger than the threshold value will be qualified of further branching. This criterion is reasonable because in general, finer mesh is required to capture the structural details if smaller-sized features were involved, and the computational cost can significantly increase. Additionally, manufacturing process planning could be over-complicated if a large number of small-sized features are involved. Therefore, the feature volume criterion is adopted in this work to verify the eligibility of feature branching. Then, another issue could be raised about selection of the appropriate threshold feature volume. Generally, a smaller value leads to more feature primitives in the resulting design and thus better mechanical performance. A larger value leads to fewer feature primitives and hence better manufacturability. This balance will be further investigated in the following numerical case study section.

5. Numerical examples

A few numerical examples will be studied in this section to demonstrate the effect of involving modeling history topological changes. In all examples, the solid material employs a Young's modulus of 1 and Poisson's ratio of 0.3.

5.1 Switching topological change

In the first example, the design domain has the size of 80*50*12.5. The input CAD model geometry is shown in Fig.12. Here, the design domain is defined as the smallest rectangular envelope fully containing the part. The part will be optimized for compliance minimization while reducing 25% of the weight. Given

the boundary conditions, the four through holes at corners are clamped and uniform pressure forces of total magnitude 1.2 are applied to the blue colored areas.

As demonstrated in Fig. 12, the part can be identically constructed with the same set of features but different sequences of Boolean operations (modeling histories). To demonstrate the effect of including the MHTD, a few different optimization scenarios will be explored. (i) First, a simple implementation with modeling history 1 is performed without considering modeling history topological change. The optimization result is shown in Fig. 13a. (ii) Then, another optimization is performed with modeling history 1 and the MHTD-driven modeling history changes. The optimized design and the resulting modeling history are presented in Fig. 13b. One modeling history topological change happens to switch the difference and union operations at the bottom layers of the hierarchical tree structure. The resulting objective is smaller than that of the first scenario. (iii) Finally, one more optimization result is derived with modeling history 2 and the MHTD-driven modeling history changes. The optimized design and the resulting modeling history are shown in Fig. 13c. As demonstrated, the modeling history keeps consistent throughout the optimization and optimization result is nearly identical to that of the second scenario.

Hence, in summary of the explored scenarios, using MHTD resolves the modeling history dependency issue wherein an identical optimization result can be derived regardless of the initial guesses.

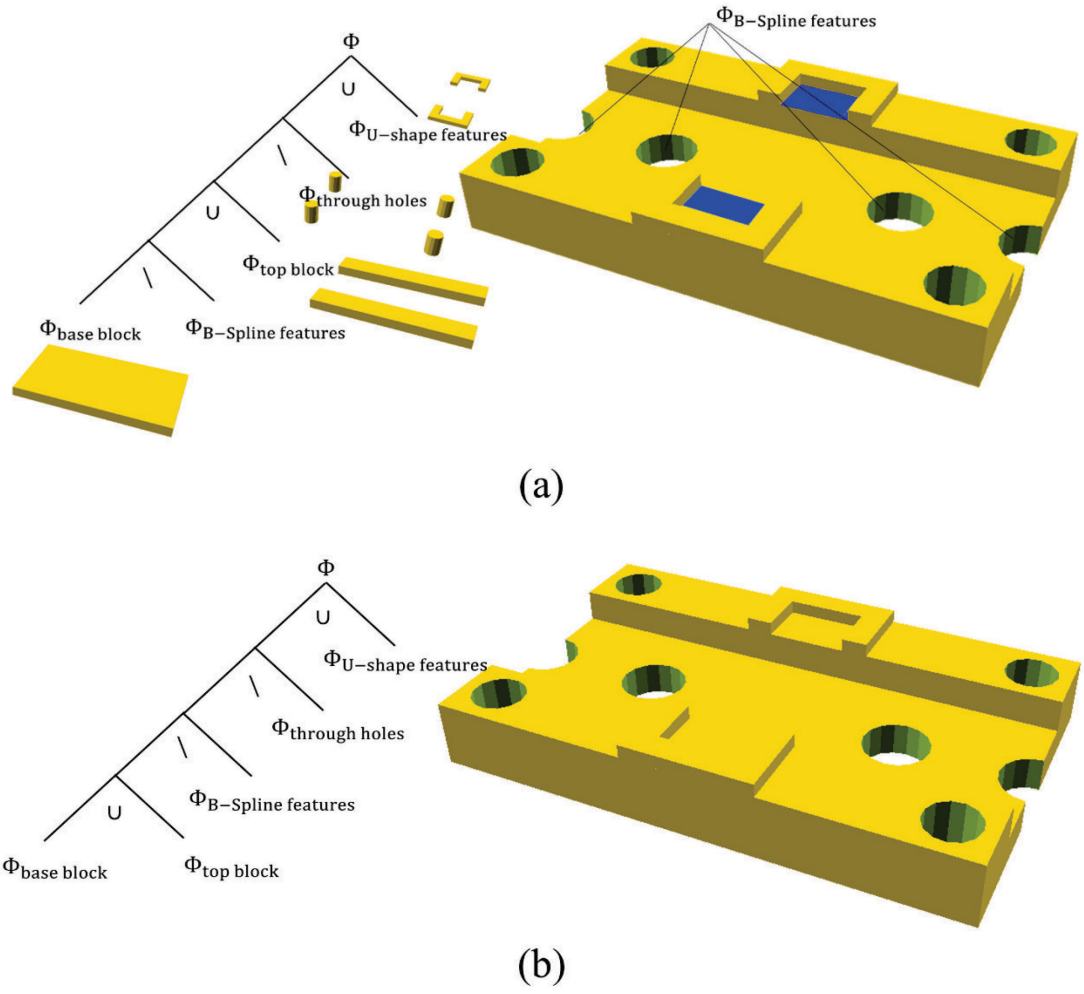

Fig. 12 The original CAD model constructed with different modeling histories: (a) Modeling history 1; (b) Modeling history 2

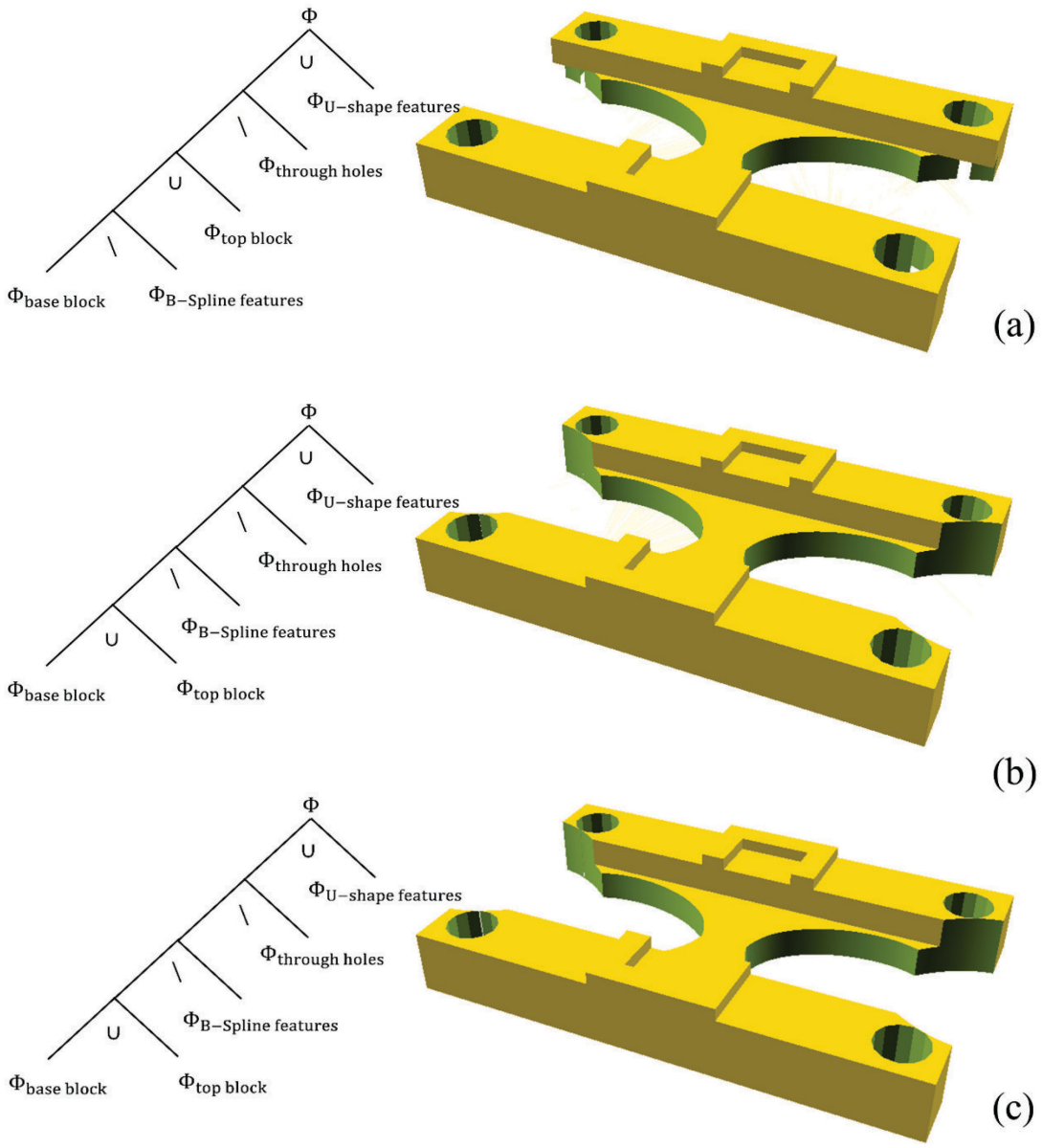

Fig. 13 Optimization results: (a) Optimization result starting with modeling history 1: modeling history topological change is not enabled (objective value = 2.12); (b) Optimization result starting with modeling history 1: modeling history topological change is enabled (objective value = 2.10); (c) Optimization result starting with modeling history 2: modeling history topological change is enabled (objective value = 2.10)

5.2 Branching topological change

In this example, the input CAD model to optimize is shown in Fig. 14. The design domain has the overall size of 85*30*10. Similarly, the design domain is defined as the smallest rectangular envelope containing the part. About the boundary condition, a lift force of magnitude 0.5 is loaded to the left end of the part; the assembly hole (in red color) at the right end is fixed with zero displacement. The part will be optimized to weigh 50% of the design domain while pursuing the highest stiffness.

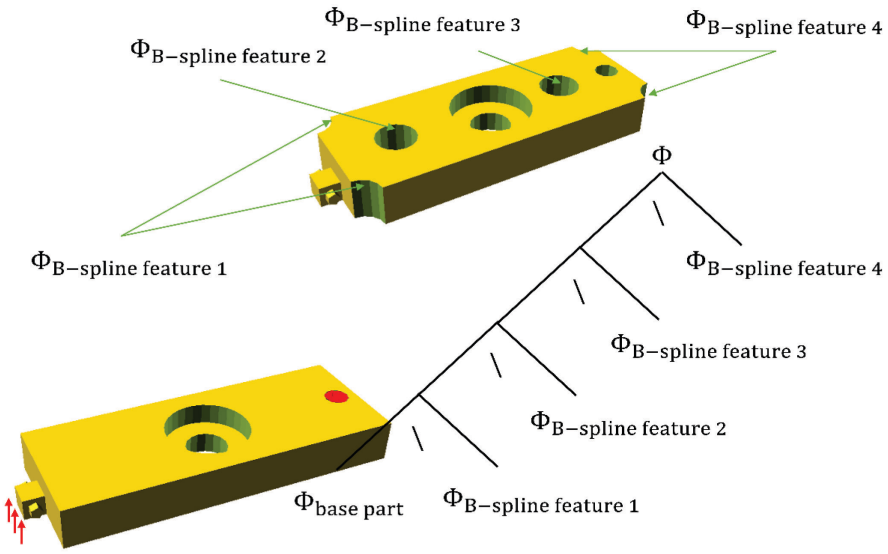

Fig. 14 The input CAD model to optimize

As discussed earlier in Sub-Section 4.2, the feature volume criterion is adopted to verify the eligibility of feature branching. In other words, B-spline features that have the feature volume larger than the threshold value will be divided into two sub-features in the extrusion direction. Hence, selection of the threshold value plays a key role in determining the finally derived part complexity. To explore this effect, the part will be optimized with three different threshold values: 25%, 15%, and 5% of the design domain volume. The optimization results are demonstrated in Fig. 15.

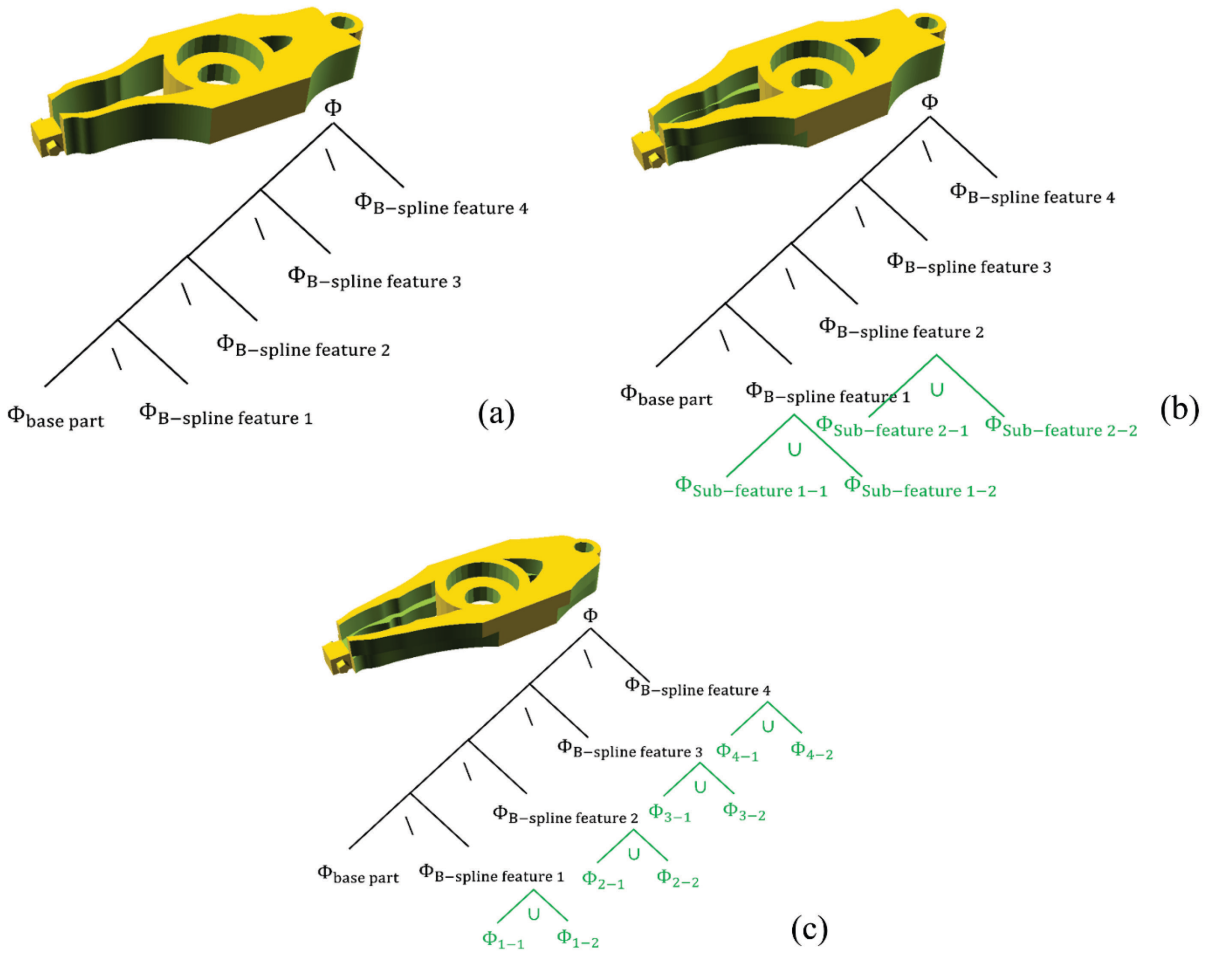

Fig. 15 Optimization results with different threshold values for feature branching: (a) Optimization result with threshold value of 25% of the total volume (obj. = 65.63); (b) Optimization result with threshold value of 15% of the total volume (obj. = 64.98); (c) Optimization result with threshold value of 5% of the total volume (obj. = 62.46)

The optimization results provide the clear clue that, by reducing the threshold value for feature branching, more sub-feature primitives are introduced into the optimization result. Accordingly, a better local optimum could be derived owing to the expanded design space. Owing to the branching modeling history change, the optimization could start from a simple geometry but end up with something complex.

5.3 A case with both kinds of modeling history topological changes

In this example, the input CAD model to optimize is shown in Fig. 16. The design domain has the overall size of 60*40*30. As demonstrated, a relatively complex modeling history is employed to build this model. Therefore, both switching and branching topological changes will be involved in this case. About the boundary condition, a force of magnitude 2 is loaded to the right-top hole (as shown by the red arrow), and the four assembly holes at corners are fixed with zero displacement. The part will be optimized to reduce 60% of its weight while maintaining the highest stiffness.

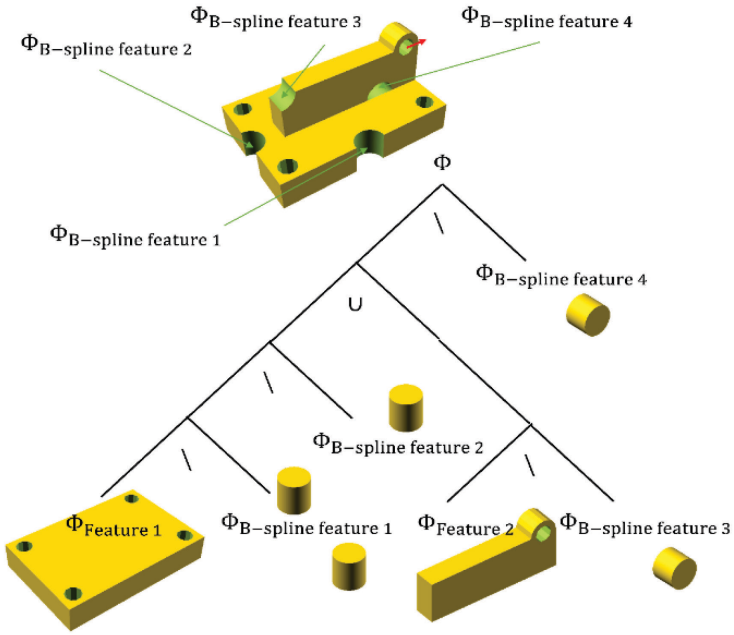

Fig. 16 The input CAD model to optimize

Then, the optimization is performed with two different setups: without and with modeling history topological changes. In the latter case, the feature volume threshold value for branching operation is 20% of the initial part volume, i.e., B-spline features that have the feature volume larger than the threshold value will be divided into two sub-features in the extrusion direction. Correspondingly, the optimization results are demonstrated in Fig. 17.

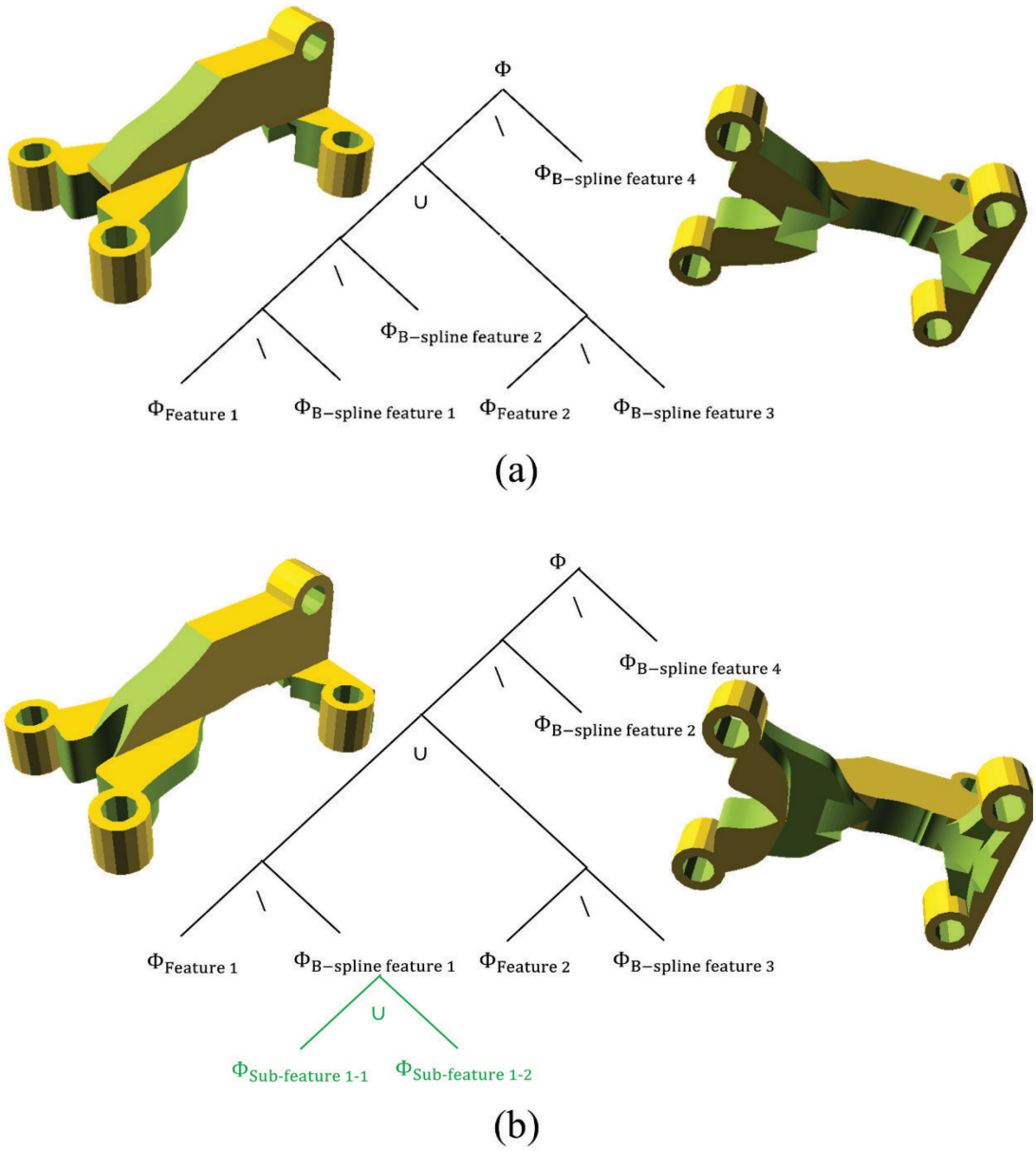

Fig. 17 Optimization results with different problem setups: (a) Optimization result without modeling history topological change (obj. = 5.70); (b) Optimization result with modeling history topological change (obj. = 5.45)

As demonstrated in Fig. 17, both switching and branching modeling history topological changes happen during the structural evolution. An objective value reduction of 4.39% has been observed due to the enabled modeling history changes. Similar conclusions can be drawn from this example, which once again confirms

the benefits of enabling modeling history topological changes. At the end, the convergence history of topology optimization with modeling history topological changes is plotted in Fig. 18. About the computing time, the result of Fig. 17 takes 107 iterations to converge, which consumes 3317s with Matlab R2011a. The mesh size is 60*20*30. A desktop computer with Intel Core i5-7400 CPU and 8GB RAM is used. Like many conventional algorithms, more than 90% of the computing time is spent on the finite element analysis.

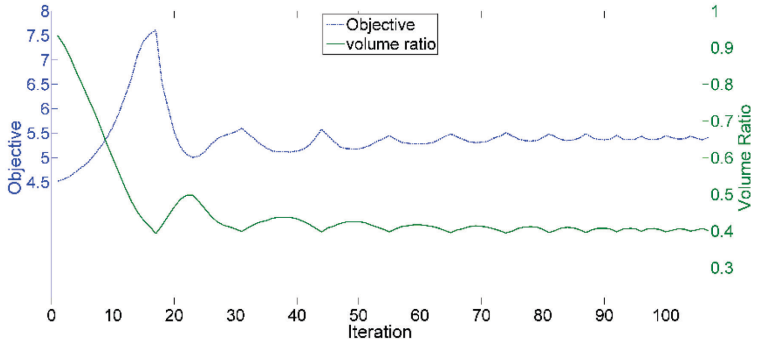

Fig. 18 Convergence history of topology optimization with modeling history topological changes

6. Conclusion

A CAD-based topology optimization system considering modeling history has been developed in this research. This system bridges the gap between CAD and topology optimization tools through macro file based information communication. B-spline based topology optimization is performed to trivialize the pre- and post-processing. More importantly, modeling history is incorporated in the topology optimization algorithm to have the history-based CAD model as design output. The key benefit is that this system could maintain as much information as possible from the original CAD model; post-editing of the topologically optimized CAD model is convenient since this system outputs the CAD model in its original format. Beyond that, the enabled modeling history topological changes expands the design space and removes the initial guess-dependency issue. Therefore, a better optimal solution could be derived than that with a fixed modeling history, just as proved by the numerical examples.

On the other hand, this is still the early study of this system. Just as the traditional CAD-CAE integration, there are still challenging issues to address. For instance, currently, only the parametric feature information and the modeling history were considered with the integrated optimization framework. More importantly, there could have more design intent stored in the original CAD model in different forms, such as geometric constraints and semantic properties. Interpretation of the geometric constraints and semantic properties would complicate the optimization problem. For instance, the property of including a coating layer would make the optimization algorithm challenging to solve. Therefore, completing the full integration will be explored in our following work.

Acknowledgement

The authors would like to acknowledge the support from National Science Foundation (CMMI-1634261) and the support from Qilu Young Scholar award, Shandong University.

References

[1] M.P. Bendsøe, N. Kikuchi, Generating optimal topologies in structural design using a homogenization method, Comput. Methods Appl. Mech. Eng. 71 (1988) 197–224. doi:10.1016/0045-7825(88)90086-2.
[2] M.P. Bendsøe, O. Sigmund, Topology Optimization, Springer Berlin Heidelberg, Berlin, Heidelberg, 2004. http://link.springer.com/10.1007/978-3-662-05086-6 (accessed May 27, 2016).
[3] X. Guo, W. Zhang, W. Zhong, Stress-related topology optimization of continuum structures involving multi-phase materials, Comput. Methods Appl. Mech. Eng. 268 (2014) 632–655. doi:10.1016/j.cma.2013.10.003.
[4] A.M. Mirzendehdel, K. Suresh, A Pareto-Optimal Approach to Multimaterial Topology Optimization, J. Mech. Des. 137 (2015) 101701. doi:10.1115/1.4031088.
[5] P. Vogiatzis, S. Chen, X. Wang, T. Li, L. Wang, Topology optimization of multi-material negative Poisson's ratio metamaterials using a reconciled level set method, Comput.-Aided Des. 83 (2017) 15–32. doi:10.1016/j.cad.2016.09.009.

[6] J. Liu, Y. Ma, A new multi-material level set topology optimization method with the length scale control capability, Comput. Methods Appl. Mech. Eng. 329 (2018) 444–463. doi:10.1016/j.cma.2017.10.011.
[7] X. Yang, M. Li, Discrete multi-material topology optimization under total mass constraint, Comput.-Aided Des. 102 (2018) 182–192. doi:10.1016/j.cad.2018.04.023.
[8] W. Zhang, J. Song, J. Zhou, Z. Du, Y. Zhu, Z. Sun, X. Guo, Topology optimization with multiple materials via moving morphable component (MMC) method, Int. J. Numer. Methods Eng. 113 (2018) 1653–1675. doi:10.1002/nme.5714.
[9] H. Kazemi, A. Vaziri, J.A. Norato, Topology Optimization of Structures Made of Discrete Geometric Components With Different Materials, J. Mech. Des. 140 (2018) 111401(1–11). doi:10.1115/1.4040624.
[10] Y. Wang, Z. Kang, Structural shape and topology optimization of cast parts using level set method, Int. J. Numer. Methods Eng. 111 (2017). doi:10.1002/nme.5503.
[11] Q. Li, W. Chen, S. Liu, H. Fan, Topology optimization design of cast parts based on virtual temperature method, Comput.-Aided Des. 94 (2018) 28–40. doi:10.1016/j.cad.2017.08.002.
[12] E.M. Dede, S.N. Joshi, F. Zhou, Topology Optimization, Additive Layer Manufacturing, and Experimental Testing of an Air-Cooled Heat Sink, J. Mech. Des. 137 (2015) 111403. doi:10.1115/1.4030989.
[13] K. Maute, A. Tkachuk, J. Wu, H. Jerry Qi, Z. Ding, M.L. Dunn, Level Set Topology Optimization of Printed Active Composites, J. Mech. Des. 137 (2015) 111402. doi:10.1115/1.4030994.
[14] J. Liu, Y. Zheng, Y. Ma, A. Qureshi, R. Ahmad, A Topology Optimization Method for Hybrid Subtractive–Additive Remanufacturing, Int. J. Precis. Eng. Manuf.-Green Technol. (2019). doi:10.1007/s40684-019-00075-8.
[15] A.T. Gaynor, J.K. Guest, Topology optimization considering overhang constraints: Eliminating sacrificial support material in additive manufacturing through design, Struct. Multidiscip. Optim. 54 (2016) 1157–1172. doi:10.1007/s00158-016-1551-x.
[16] A.M. Mirzendehdel, K. Suresh, Support structure constrained topology optimization for additive manufacturing, Comput.-Aided Des. 81 (2016) 1–13. doi:10.1016/j.cad.2016.08.006.
[17] J. Liu, A.C. To, Deposition path planning-integrated structural topology optimization for 3D additive manufacturing subject to self-support constraint, Comput.-Aided Des. 91 (2017) 27–45. doi:10.1016/j.cad.2017.05.003.
[18] X. Guo, J. Zhou, W. Zhang, Z. Du, C. Liu, Y. Liu, Self-supporting structure design in additive manufacturing through explicit topology optimization, Comput. Methods Appl. Mech. Eng. 323 (2017) 27–63. doi:10.1016/j.cma.2017.05.003.
[19] M.E. Orme, M. Gschweitl, M. Ferrari, I. Madera, F. Mouriaux, Designing for Additive Manufacturing: Lightweighting Through Topology Optimization Enables Lunar Spacecraft, J. Mech. Des. 139 (2017) 100905(1–6). doi:10.1115/1.4037304.
[20] M.J. Geiss, N. Boddeti, O. Weeger, K. Maute, M.L. Dunn, Combined Level-Set-XFEM-Density Topology Optimization of 4D Printed Structures undergoing Large Deformation, J. Mech. Des. (2018). doi:10.1115/1.4041945.
[21] J. Liu, Y. Zheng, R. Ahmad, J. Tang, Y. Ma, Minimum length scale constraints in multi-scale topology optimisation for additive manufacturing, Virtual Phys. Prototyp. 14 (2019) 229–241. doi:10.1080/17452759.2019.1584944.
[22] H. Yu, J. Huang, B. Zou, W. Shao, J. Liu, Stress-constrained shell-lattice infill structural optimization for additive manufacturing, Virtual Phys. Prototyp. (2019). doi:10.1080/17452759.2019.1647488.
[23] S. Chen, W. Chen, S. Lee, Level set based robust shape and topology optimization under random field uncertainties, Struct. Multidiscip. Optim. 41 (2010) 507–524. doi:10.1007/s00158-009-0449-2.
[24] S. Chen, W. Chen, A new level-set based approach to shape and topology optimization under geometric uncertainty, Struct. Multidiscip. Optim. 44 (2011) 1–18. doi:10.1007/s00158-011-0660-9.

[25] X. Guo, W. Zhang, L. Zhang, Robust structural topology optimization considering boundary uncertainties, Comput. Methods Appl. Mech. Eng. 253 (2013) 356–368. doi:10.1016/j.cma.2012.09.005.
[26] X. Guo, X. Zhao, W. Zhang, J. Yan, G. Sun, Multi-scale robust design and optimization considering load uncertainties, Comput. Methods Appl. Mech. Eng. 283 (2015) 994–1009. doi:10.1016/j.cma.2014.10.014.
[27] S.-H. Ha, H.Y. Lee, K. Hemker, J.K. Guest, Topology Optimization of 3D Woven Materials using a Ground Structure Design Variable Representation, J. Mech. Des. (2018). doi:10.1115/1.4042114.
[28] W. Zhang, Y. Liu, Z. Du, Y. Zhu, X. Guo, A Moving Morphable Component Based Topology Optimization Approach for Rib-Stiffened Structures Considering Buckling Constraints, J. Mech. Des. 140 (2018) 111404(1–12). doi:10.1115/1.4041052.
[29] M. Bremicker, M. Chirehdast, N. Kikuchi, P.Y. Papalambros, Integrated Topology and Shape Optimization in Structural Design∗, Mech. Struct. Mach. 19 (1991) 551–587. doi:10.1080/08905459108905156.
[30] C.-Y. Lin, L.-S. Chao, Automated image interpretation for integrated topology and shape optimization, Struct. Multidiscip. Optim. 20 (2000) 125–137. doi:10.1007/s001580050144.
[31] A.R. Yildiz, N. Öztürk, N. Kaya, F. Öztürk, Integrated optimal topology design and shape optimization using neural networks, Struct. Multidiscip. Optim. 25 (2003) 251–260. doi:10.1007/s00158-003-0300-0.
[32] K. Maute, E. Ramm, Adaptive topology optimization, Struct. Optim. 10 (1995) 100–112. doi:10.1007/BF01743537.
[33] S.-K. Youn, S.-H. Park, A study on the shape extraction process in the structural topology optimization using homogenized material, Comput. Struct. 62 (1997) 527–538. doi:10.1016/S0045-7949(96)00217-9.
[34] M.-H. Hsu, Y.-L. Hsu, Interpreting three-dimensional structural topology optimization results, Comput. Struct. 83 (2005) 327–337. doi:10.1016/j.compstruc.2004.09.005.
[35] Y.-L. Hsu, M.-S. Hsu, C.-T. Chen, Interpreting results from topology optimization using density contours, Comput. Struct. 79 (2001) 1049–1058. doi:10.1016/S0045-7949(00)00194-2.
[36] A. Koguchi, N. Kikuchi, A surface reconstruction algorithm for topology optimization, Eng. Comput. 22 (2006) 1–10. doi:10.1007/s00366-006-0023-0.
[37] K.-H. Chang, P.-S. Tang, Integration of design and manufacturing for structural shape optimization, Adv. Eng. Softw. 32 (2001) 555–567. doi:10.1016/S0965-9978(00)00103-4.
[38] J. Liu, Y. Ma, A survey of manufacturing oriented topology optimization methods, Adv. Eng. Softw. 100 (2016) 161–175. doi:10.1016/j.advengsoft.2016.07.017.
[39] E. Cervera, J. Trevelyan, Evolutionary structural optimisation based on boundary representation of NURBS. Part I: 2D algorithms, Comput. Struct. 83 (2005) 1902–1916. doi:10.1016/j.compstruc.2005.02.016.
[40] E. Cervera, J. Trevelyan, Evolutionary structural optimisation based on boundary representation of NURBS. Part II: 3D algorithms, Comput. Struct. 83 (2005) 1917–1929. doi:10.1016/j.compstruc.2005.02.017.
[41] W. Zhang, W. Yang, J. Zhou, D. Li, X. Guo, Structural Topology Optimization Through Explicit Boundary Evolution, J. Appl. Mech. 84 (2016) 011011. doi:10.1115/1.4034972.
[42] W. Zhang, J. Chen, X. Zhu, J. Zhou, D. Xue, X. Lei, X. Guo, Explicit three dimensional topology optimization via Moving Morphable Void (MMV) approach, Comput. Methods Appl. Mech. Eng. 322 (2017) 590–614. doi:10.1016/j.cma.2017.05.002.
[43] W. Zhang, L. Zhao, T. Gao, S. Cai, Topology optimization with closed B-splines and Boolean operations, Comput. Methods Appl. Mech. Eng. 315 (2017) 652–670. doi:10.1016/j.cma.2016.11.015.
[44] W. Zhang, L. Zhao, T. Gao, CBS-based topology optimization including design-dependent body loads, Comput. Methods Appl. Mech. Eng. 322 (2017) 1–22. doi:10.1016/j.cma.2017.04.021.

[45] W. Zhang, D. Li, J. Zhou, Z. Du, B. Li, X. Guo, A Moving Morphable Void (MMV)-based explicit approach for topology optimization considering stress constraints, Comput. Methods Appl. Mech. Eng. 334 (2018) 381–413. doi:10.1016/j.cma.2018.01.050.
[46] J. Liu, A.T. Gaynor, S. Chen, Z. Kang, K. Suresh, A. Takezawa, L. Li, J. Kato, J. Tang, C.C.L. Wang, L. Cheng, X. Liang, A.C. To, Current and future trends in topology optimization for additive manufacturing, Struct. Multidiscip. Optim. 57 (2018) 2457–2483. doi:10.1007/s00158-018-1994-3.
[47] J. Liu, Y. Ma, Sustainable Design-Oriented Level Set Topology Optimization, J. Mech. Des. 139 (2017) 011403 (1–8). doi:10.1115/1.4035052.
[48] J. Liu, Y.-S. Ma, 3D level-set topology optimization: a machining feature-based approach, Struct. Multidiscip. Optim. 52 (2015) 563–582. doi:10.1007/s00158-015-1263-7.
[49] Y. Mei, X. Wang, G. Cheng, A feature-based topological optimization for structure design, Adv. Eng. Softw. 39 (2008) 71–87. doi:10.1016/j.advengsoft.2007.01.023.
[50] J. Zhu, W. Zhang, P. Beckers, Y. Chen, Z. Guo, Simultaneous design of components layout and supporting structures using coupled shape and topology optimization technique, Struct. Multidiscip. Optim. 36 (2008) 29–41. doi:10.1007/s00158-007-0155-x.
[51] W. Zhang, L. Xia, J. Zhu, Q. Zhang, Some Recent Advances in the Integrated Layout Design of Multicomponent Systems, J. Mech. Des. 133 (2011) 104503–104503. doi:10.1115/1.4005083.
[52] M. Zhou, M.Y. Wang, Engineering feature design for level set based structural optimization, Comput.-Aided Des. 45 (2013) 1524–1537. doi:10.1016/j.cad.2013.06.016.
[53] L. Xia, J. Zhu, W. Zhang, P. Breitkopf, An implicit model for the integrated optimization of component layout and structure topology, Comput. Methods Appl. Mech. Eng. 257 (2013) 87–102. doi:10.1016/j.cma.2013.01.008.
[54] W. Zhang, W. Zhong, X. Guo, Explicit layout control in optimal design of structural systems with multiple embedding components, Comput. Methods Appl. Mech. Eng. 290 (2015) 290–313. doi:10.1016/j.cma.2015.03.007.
[55] Z. Kang, Y. Wang, Y. Wang, Structural topology optimization with minimum distance control of multiphase embedded components by level set method, Comput. Methods Appl. Mech. Eng. 306 (2016) 299–318. doi:10.1016/j.cma.2016.04.001.
[56] Y. Zhou, W. Zhang, J. Zhu, Z. Xu, Feature-driven topology optimization method with signed distance function, Comput. Methods Appl. Mech. Eng. 310 (2016) 1–32. doi:10.1016/j.cma.2016.06.027.
[57] W. Zhang, Y. Zhou, J. Zhu, A comprehensive study of feature definitions with solids and voids for topology optimization, Comput. Methods Appl. Mech. Eng. 325 (2017) 289–313. doi:10.1016/j.cma.2017.07.004.
[58] G.-H. Choi, D. Mun, S. Han, Exchange of CAD part models based on the macro-parametric approach, Int. J. CadCam. 2 (2002) 13–21.
[59] S.H. Farjana, S. Han, D. Mun, Implementation of persistent identification of topological entities based on macro-parametrics approach, J. Comput. Des. Eng. 3 (2016) 161–177. doi:10.1016/j.jcde.2016.01.001.
[60] J. Yang, S. Han, J. Cho, B. Kim, H.Y. Lee, An XML-Based Macro Data Representation for a Parametric CAD Model Exchange, Comput.-Aided Des. Appl. 1 (2004) 153–162. doi:10.1080/16864360.2004.10738254.
[61] D. Mun, S. Han, J. Kim, Y. Oh, A set of standard modeling commands for the history-based parametric approach, Comput.-Aided Des. 35 (2003) 1171–1179. doi:10.1016/S0010-4485(03)00022-8.
[62] M.T.H. Khan, F. Demoly, K.-Y. Kim, Formal ontology and CAD integration with macro parametric approach, Comput.-Aided Des. Appl. 14 (2017) 24–32. doi:10.1080/16864360.2017.1308078.
[63] J. Chen, V. Shapiro, K. Suresh, I. Tsukanov, Shape optimization with topological changes and parametric control, Int. J. Numer. Methods Eng. 71 (2007) 313–346. doi:10.1002/nme.1943.
[64] M.Y. Wang, X. Wang, D. Guo, A level set method for structural topology optimization, Comput. Methods Appl. Mech. Eng. 192 (2003) 227–246. doi:10.1016/S0045-7825(02)00559-5.

[65] G. Allaire, F. Jouve, A.-M. Toader, Structural optimization using sensitivity analysis and a level-set method, J. Comput. Phys. 194 (2004) 363–393. doi:10.1016/j.jcp.2003.09.032.
[66] M. Burger, B. Hackl, W. Ring, Incorporating topological derivatives into level set methods, J. Comput. Phys. 194 (2004) 344–362. doi:10.1016/j.jcp.2003.09.033.
[67] J. Sokolowski, A. Zochowski, On the Topological Derivative in Shape Optimization, SIAM J. Control Optim. 37 (1999) 1251–1272. doi:10.1137/S0363012997323230.
[68] J. Céa, S. Garreau, P. Guillaume, M. Masmoudi, The shape and topological optimizations connection, Comput. Methods Appl. Mech. Eng. 188 (2000) 713–726. doi:10.1016/S0045-7825(99)00357-6.

List of figure captions

Fig. 1 System framework

Fig. 2 Modeling history topological change

Fig. 3 Script-based CAD modeling in OpenSCAD: (a) Modeling script; (b) CAD model; (c) Modeling history

Fig. 4 Quadratic B-spline basis functions ($n = 6, k = 2$) with the knot vector of: (a) $\mathbf{T} = [0,0,0,0.2,0.4,0.6,0.8,1,1,1]$ and (b) $\mathbf{T} = [0,0,0,0.3,0.4,0.6,0.7,1,1,1]$

Fig. 5 Closed B-spline

Fig. 6 Constructive description of the bracket

Fig. 7 Initial guess of the topology optimization problem: (a) Design domain and boundary conditions (only the front half is demonstrated of size 60*30*5); (b) Initially deployed machining features; (c) The closed B-spline curves in 2D view

Fig. 8 The topology optimization result (objective value = 13.47): (a) Initially deployed machining features; (b) The closed B-spline curves in 2D view

Fig. 9 Optimization with a fixed modeling history

Fig. 10 Optimization with Boolean operation switch

Fig. 11 Illustration of the branching topological change

Fig. 12 The original CAD model constructed with different modeling histories: (a) Modeling history 1; (b) Modeling history 2

Fig. 13 Optimization results: (a) Optimization result starting with modeling history 1: modeling history topological change is not enabled (objective value = 2.12); (b) Optimization result starting with modeling

history 1: modeling history topological change is enabled (objective value = 2.10); (c) Optimization result starting with modeling history 2: modeling history topological change is enabled (objective value = 2.10)

Fig. 14 The input CAD model to optimize

Fig. 15 Optimization results with different threshold values for feature branching: (a) Optimization result with threshold value of 25% of the total volume (obj. = 65.63); (b) Optimization result with threshold value of 15% of the total volume (obj. = 64.98); (c) Optimization result with threshold value of 5% of the total volume (obj. = 62.46)

Fig. 16 The input CAD model to optimize

Fig. 17 Optimization results with different problem setups: (a) Optimization result without modeling history topological change (obj. = 5.70); (b) Optimization result with modeling history topological change (obj. = 5.45)

Fig. 18 Convergence history of topology optimization with modeling history topological changes